Advances in Science and Technology Research Journal

Advances in Science and Technology Research Journal, 2026, 20(3), 197–212
https://doi.org/10.12913/22998624/213998
ISSN 2299-8624, License CC-BY 4.0

Received: 2025.09.29
Accepted: 2025.11.05
Published: 2026.02.01

Parametric numerical study on the seismic performance of beam-to-double-skin concrete-filled steel tubular column connections

Ameer Baiee[1*]

[1] Department of civil engineering, College of Engineering, University of Babylon, Babylon, Iraq
* Corresponding author's e-mail: eng.ameer.tuama@uobabylon.edu.iq

ABSTRACT

Earthquakes are natural phenomena that can cause significant human and financial damage, making the design of earthquake-resistant buildings crucial. Beam-to-column connections are vital in any structure, and further research is needed to understand the parameters influencing their behavior. This is especially important in buildings with double-skin concrete-filled steel tubular columns (DSCFT). The aim of this study was to explore the impact of void percentage, concrete strength, and inner skin thickness on beam-to-DSCFT column connections. After validating numerical modeling, three model groups with eleven models were analyzed under cyclical loading. Results indicate that increasing the void percentage in the column from 10% to 100% reduces the maximum tolerable moment from 519.49 to 354.64 kN.m, changes rupture mode from tensile to buckling, and decreases cumulative dissipated energy. Conversely, increasing concrete strength from 20 MPa to 70 MPa raises the maximum tolerable moment from 507.698 to 524.24 kN.m, with a cumulative increase in dissipated energy. Additionally, increasing the inner skin thickness from 5 mm to 15 mm raises the maximum tolerable moment from 506.978 to 520.892 kN.m, while reducing cumulative dissipated energy.

Keywords: DSCFT column, seismic behavior, anchor-rotation diagram, stress contour, inner skin thickness, column middle void percentage.

INTRODUCTION

In recent years, composite columns have gained significant attention in the construction industry due to their cost-effectiveness and excellent seismic ductility behavior [1–3]. Concurrently, steel columns encased with concrete offer enhanced ductility, stemming from the confinement of concrete and higher hardness, while also providing substantial cost savings [4]. A notable example of composite columns is the double-skin concrete-filled steel tubular column (DSCFT), which presents numerous benefits [5, 6], such as high thermal resistance, superior ductility, and exceptional energy absorption capacity. Furthermore, the elimination of the need for formwork during concrete pouring results in both time and cost savings. These advantages have led to the widespread adoption of DSCFT columns in civil engineering applications [7–11]. Figure 1 illustrates two common configurations of DSCFT columns, namely circular and square profiles.

One of the critical aspects concerning DSCFT columns is the connections utilized in these columns [12, 13]. The connection must be designed in a manner that allows both steel and concrete to effectively participate in load-bearing. Additionally, the plastic connection should form in the beam, fulfilling the condition of a weak beam and strong column, ensuring that the connection has sufficient grip [14–17]. The inclusion of concrete in a CFT column significantly enhances both the initial and post-yield stiffness. The concrete in this configuration contributes to adequate stiffness at the column corners and prevents excessive movement within the column wall [18, 19].

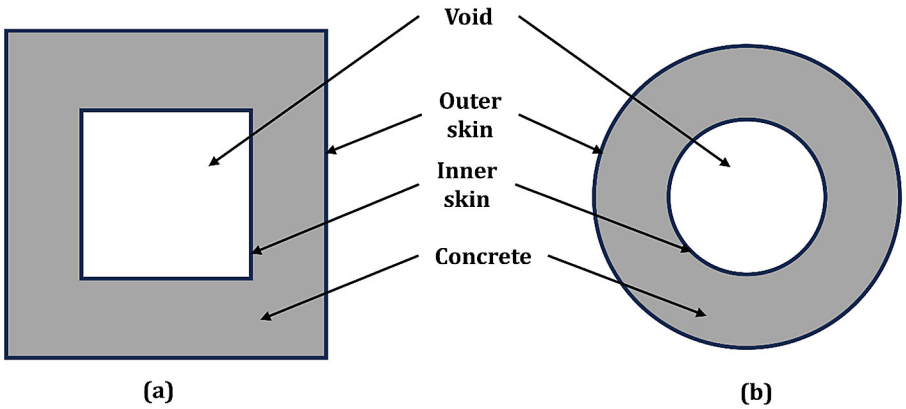

Figure 1. Common DSCFT cross section configurations (a) Square, (b) Circular

Over the past two decades, significant economic and human losses have occurred due to structural collapses during earthquakes [20]. Consequently, substantial efforts have been made by researchers to develop earthquake-resistant systems. In particular, extensive studies have been carried out on the behavior of flexural connections in CFT columns under cyclic loading, leading to the introduction of new connection designs and the development of corresponding standards.

In 2016, Hassan et al. [21] investigated the connection between the beam and a DSCFT column. Two years later, Dongfang Zhang et al. [22] conducted both numerical and experimental studies on this connection. Their research involved subjecting four half-scale models to cyclic loading, studying their hysteresis behavior and failure modes, and subsequently examining numerical models using the finite element method after validation. In 2020, Hu et al. [23] carried out an experimental study of a steel frame with a DSCFT column and a composite shear wall. In 2022, Zhou et al. [24] explored an experimental investigation of beam-to-DSCFT column connections using special materials. Additionally, in 2022, Phan et al. [25] studied the numerical connection of the beam to a DSCFT column, using UHPC concrete for its construction.

Given that the structural members of composite cross-sectional buildings are frequently exposed to damage under seismic loading, further research is essential to gain a comprehensive understanding of the performance of these components during earthquakes. Therefore, in this study, after reviewing relevant literature and valid sources, numerical modeling validation was conducted in the Abacus software. Following this, three groups of numerical models were analyzed in the Abacus software under cyclic loading. The study concludes with a comparison of the maximum moment before tolerance, the dissipated energy, and the rupture behavior of the numerical models.

VALIDATION

To verify the accuracy of the numerical model, the experimental study conducted by Vulcu et al. [26] was utilized. In their research, the RBS-700 experimental model, with its experimental configuration illustrated in Figure 2, was chosen for simulation using the Abacus software. Furthermore, the potential scaling effects between the half-scale experimental setup and the full-scale numerical simulations were carefully considered during the modeling process. The geometric, material, and loading parameters were adjusted according to similarity laws to ensure that the stress–strain behavior and failure mechanisms observed in the reduced-scale specimens accurately represent those expected at full scale. Moreover, validation through comparison between the experimental and numerical results confirmed the reliability of the adopted scaling approach, as the observed deviations were within acceptable engineering limits.

In the experimental setup, the beam section used was IPE400, fabricated from S460 steel, whereas the column section was RHS 300 × 300 × 12.5 mm, made of S355 steel. The structural behavior of the model was evaluated through both the push-over curve and the hysteresis response. In the numerical simulation using ABAQUS, the modeling process was carried out in several stages.

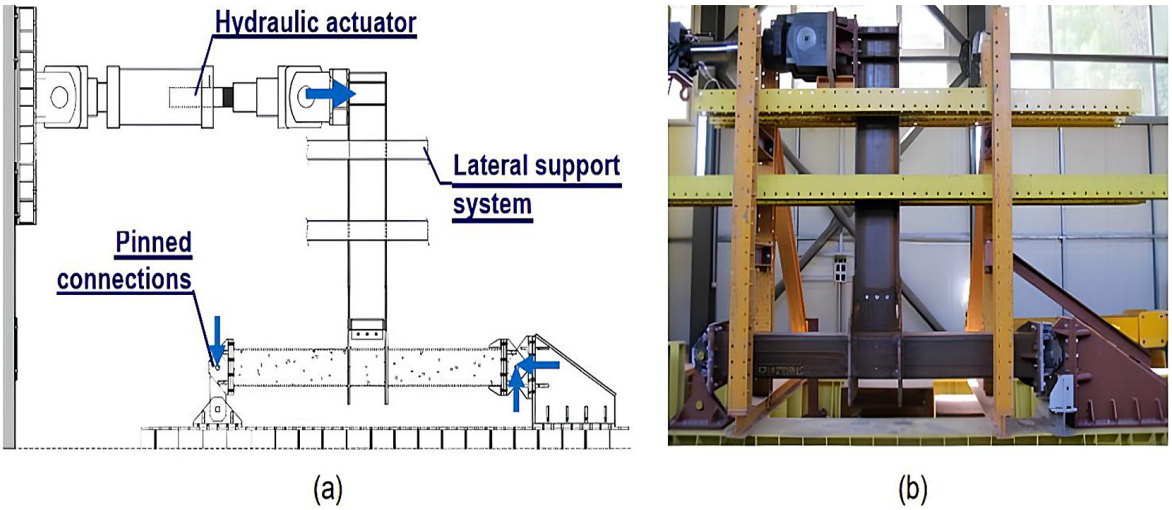

Figure 2. Experimental configuration: (a) schematic illustration; (b) laboratory test setup adapted from Vulcu et al. [26]

In the first stage, all components of the laboratory specimen were constructed according to the geometric specifications reported by Vulcu et al. [26]. In the second stage, the material properties identified in the experimental work of Vulcu et al. were defined and assigned to the respective components. A bilinear material model was adopted to simulate the behavior of steel, while the concrete damaged plasticity (CDP) model was implemented to represent both the elastic and plastic responses of concrete.

In the third stage, the individual components were assembled to form the complete model. In the fourth stage, the analysis procedure was specified, where a general static analysis was employed. Due to the computational cost and complexity associated with dynamic analysis, nonlinear static (push-over) analysis was utilized as a practical and sufficiently accurate alternative for predicting structural behavior.

In the fifth stage, the interactions between components were defined. A tie constraint was applied to simulate the welded connections between steel elements, assuming full bonding. In the sixth stage, the boundary conditions and cyclic loading protocol for the numerical models in this study were defined to exactly match the boundary conditions of the experimental specimen used for validating the numerical modeling within the same study.

In the seventh stage, In the finite element modeling performed using Abaqus software, meshing parameters were standardized across all components, with solid elements of type C3D8R (8-node linear brick with reduced integration and hourglass control) used for both concrete and steel parts, and a uniform mesh size of 50 mm adopted to ensure compatibility between adjacent components while maintaining a balance between computational efficiency and accuracy in capturing nonlinear responses. Finally, after completing the analysis, the hysteresis response of the numerical model was extracted for comparison with the experimental results. A mesh sensitivity analysis was conducted to determine the appropriate mesh size, where there are no significant changes in results with a smaller mesh. Mesh sizes of 50 mm, 45 mm, 40 mm, and 35 mm were examined for the specimens to find the suitable size. The model with a 50 mm mesh size is considered appropriate, because it reduces analysis time compared to other sizes and provides the results close to experimental findings. It should be noted that for the convergence of the analysis, the L2 norm for both force and displacement control is assumed to be equal to 0.005.

As illustrated in Figure 3, the developed finite element model shows strong agreement with the experimental observations for both the push-over and hysteresis responses, thereby confirming the accuracy, validity, and reliability of the adopted modeling methodology.

As it was shown in Figure 3, the ultimate strength of the numerical model and the laboratory specimen in hysteresis analysis is about 600 kNm and 580 kNm, respectively, which is about 3% different. Also, the ultimate strength of the numerical model and the laboratory specimen

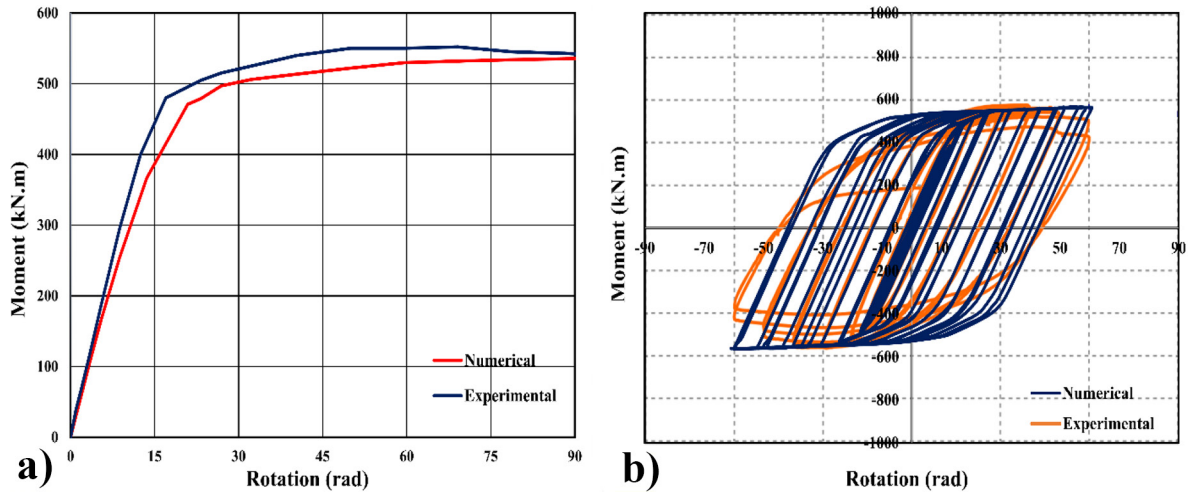

Figure 3. Comparison of numerical and experimental results: (a) Push-over analysis, (b) Hysteresis analysis

in pushover analysis is about (585 and 560) kN.m, respectively, which is about 5% different. In addition, in all models, the difference in initial stiffness is negligible. Therefore, it can be said that the numerical model results agree well with the laboratory results.

BASIC ASSUMPTIONS AND NUMERICAL MODELS

The primary objective of this study was to investigate the behavior of welded connections between steel beams and composite DSCFT columns. A total of 11 numerical models, classified into three groups as summarized in Table 1, were developed and analyzed.

In Table 1, the Specimen Label column presents the designated names for each numerical model. The letter G is derived from the word Group, and V from Void. The abbreviation Fc represents the concrete strength, while IS taken from Inner Skin.

The geometric details of the specimens, including the connection configuration, are illustrated in Figure 4. In all models, the beam cross-section is IPE400, and the outer steel tube of the DSCFT column has a square of 250 mm.

The steel components used in all numerical models were assigned the mechanical properties of ST37 steel, as detailed in Table 2.

In addition to the elastic and plastic characteristics, the Ductile Damage criterion was applied to the steel material to simulate damage accumulation under cyclic loading. This approach is supported by the previous studies that emphasize the importance of capturing stiffness degradation and strength reduction in

Table 1. Characteristics of the numerical models

Group	Specimen label	Void (%)	Fc	Steel materials	Outer skin	Beam	External diagram	Inner skin
1	G01-V10%	10	30	ST37	BO × 250 × 250 × 10	IPE 400	Yes (10 mm)	Yes (10 mm)
	G01-V25%	25	30	ST37	BO × 250 × 250 × 10	IPE 400	Yes (10 mm)	Yes (10 mm)
	G01-V50%	50	30	ST37	BO × 250 × 250 × 10	IPE 400	Yes (10 mm)	Yes (10 mm)
	G01-V100%	100	30	ST37	BO × 250 × 250 × 10	IPE 400	Yes (10 mm)	No
2	G02-Fc20	25	20	ST37	BO × 250 × 250 × 10	IPE 400	Yes (10 mm)	Yes (10 mm)
	G02-Fc30	25	30	ST37	BO × 250 × 250 × 10	IPE 400	Yes (10 mm)	Yes (10 mm)
	G02-Fc50	25	50	ST37	BO × 250 × 250 × 10	IPE 400	Yes (10 mm)	Yes (10 mm)
	G02-Fc70	25	70	ST37	BO × 250 × 250 × 10	IPE 400	Yes (10 mm)	Yes (10 mm)
3	G03-IS5	25	30	ST37	BO × 250 × 250 × 10	IPE 400	Yes (10 mm)	Yes (5 mm)
	G03-IS10	25	30	ST37	BO × 250 × 250 × 10	IPE 400	Yes (10 mm)	Yes (10 mm)
	G03-IS15	25	30	ST37	BO × 250 × 250 × 10	IPE 400	Yes (10 mm)	Yes (15 mm)

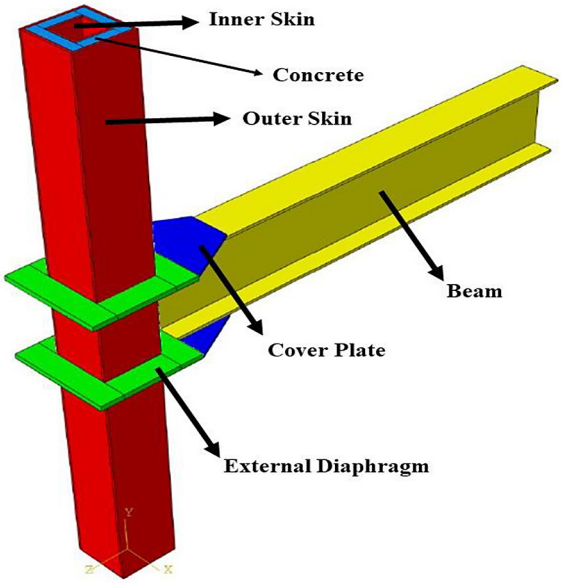

Figure 4. Geometric characteristics and details of numerical models in this research

ductile steel components subjected to repeated loading cycles [27–31].

The use of the Ductile Damage model is particularly relevant for the welded beam-to-column connections in double-layer DSCFT composite systems, which exhibit strength degradation and pinching behavior in their hysteresis response under cyclic loading. This modeling approach allows for a more accurate prediction of structural performance, especially in the scenarios involving seismic or fatigue loading conditions.

For the concrete material, the CDP model was adopted to simulate both the elastic and inelastic behavior of concrete under static and cyclic loading. This model has been widely validated and recommended for use in finite element analysis of concrete structures, especially for capturing tensile cracking, compressive crushing, and stiffness degradation under cyclic loads [32, 33]. The dilation angle for the model was set at (56°) [6]. This angle is obtained due to a change in volumetric strain resulting from plastic shearing and depends on the internal friction angle. Table 3 represents the details of concrete properties and (CDP) parameters used in the Abaqus program.

Figure 5 illustrates the definition of bending moment and rotation used in this study. The bending moment was calculated as the product of the applied lateral force at the beam tip and the horizontal distance to the centerline of the column. Correspondingly, the rotation was determined as the ratio between the measured lateral displacement at the beam tip and the same reference distance to the column centerline.

The cyclic loading protocol applied to all numerical models is shown in Figure 3. This loading was defined in accordance with the ANSI/AISC 341 standard [34], which is widely accepted for evaluating the seismic performance of structural components under repeated load reversals.

The chosen ranges for void percentage (10–100%), compressive strength of concrete (20–70 MPa), and inner steel skin thickness (5–15 mm) were selected based on a combination of experimental references [26] and practical considerations for real-world column sizes. The selected values represent typical geometric and material properties observed in medium- to large-scale composite columns. Specifically:

Table 2. Mechanical specification of ST37 steel

Density (kg/m³)	E (GPa)	Poisson ratio	Yield stress (MPa)	Ultimate stress (MPa)	Elongation (%)
7800	200	0.3	240	370	44

Table 3. Concrete peoperties and CDP parameters

Concrete properties	Young's modulus (E)	23.5 GPa
	Poission's ratio (υ)	0.2
	Specific weight (SG)	2400 Kg/m³
CDP parameters	Dilation angle (ψ)	56°
	Eccentricity (e)	0.1
	fb_0/fc_0	1.16
	The second stress invariant/tensile meridian (K)	0.667
	Viscosity parameter (μ)	0.001

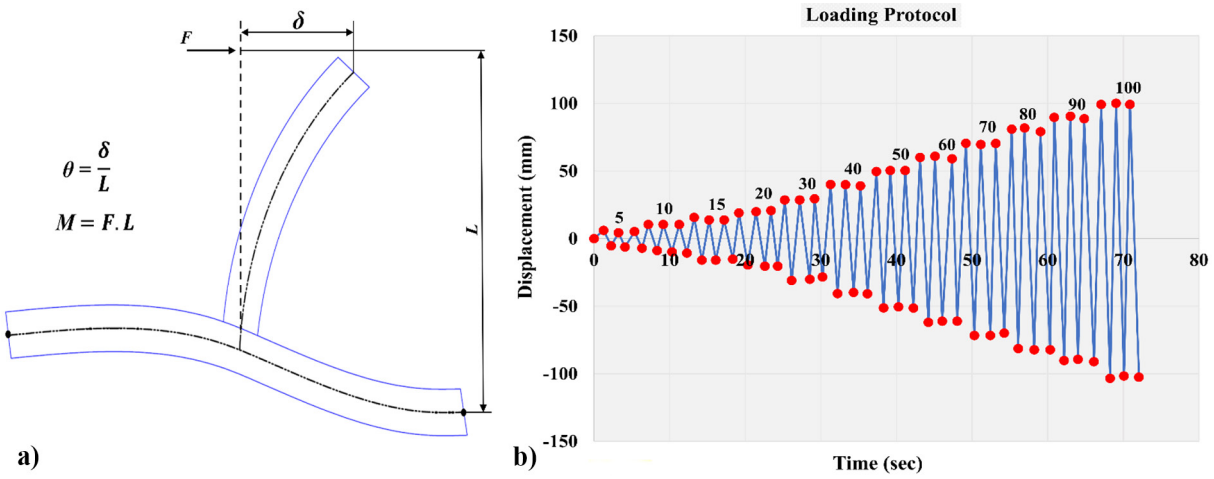

Figure 5. (a) Definition of bending and rotational anchor for beam-to-column connection assembly, (b) Loading protocol

Voids (10–100%): This range covers from nearly solid infill to fully hollow sections, allowing the study of different filler efficiencies while reflecting realistic variations in lightweight infill proportions used in practice.

Concrete strength (20–70 MPa): The range corresponds to normal to high-performance concrete commonly employed in structural columns, ensuring that the simulated columns cover the practical strength levels for design purposes.

Inner skin thickness (5–15 mm): These values represent typical internal steel tube thicknesses for composite columns of squares around 250–300 mm, as used in the experimental reference [26], providing both structural feasibility and realistic interaction with the concrete infill.

This justification ensures that the numerical models are not only parametric studies but also meaningful for practical design applications.

RESULTS INTERPRETATION AND DISCUSSION

Investigation of the effect of the void percentage in the middle of the column section

The percentage of void in the central core of the column is considered one of the key parameters influencing the seismic performance of double-layer composite columns (DSCFT). To evaluate the effect of this parameter, the first group of numerical models was specifically designed and analyzed.

As it was shown in Table 1, the selected reference models incorporate varying void ratios in the inner core of the column, including 10%, 25%, 50%, and 100%. These percentages were chosen to assess the influence of different levels of void on the structural response under cyclic loading.

Figure 6 illustrates the stress distribution and damage contours for the first group of DSCFT column models, highlighting the formation of plastic hinges and initial crack propagation zones. It also presents the stress contours and the locations of plastic strain concentration, which further clarify the influence of void ratio on stress distribution and failure mechanisms. The red areas in the figure represent the regions where plastic deformation and damage initiation occur.

As it was observed, in all models, the plastic hinge primarily forms in the beam rather than in the column, which is considered a desirable failure mechanism in seismic design. In the G01-V10% model, damage is concentrated at the upper flange of the beam near the beam-to-column junction. In the G01-V50% model, damage shifts further along the beam length, appearing below the mid-height of the section. In the G01-V100% model, plastic deformation predominantly occurs in the beam flange.

These results indicate that increasing the void ratio in the central region of the column leads to a progressive shift in the failure mechanism from tensile yielding near the top of the beam to compressive-induced buckling near the lower beam flange. In other words, as the void percentage

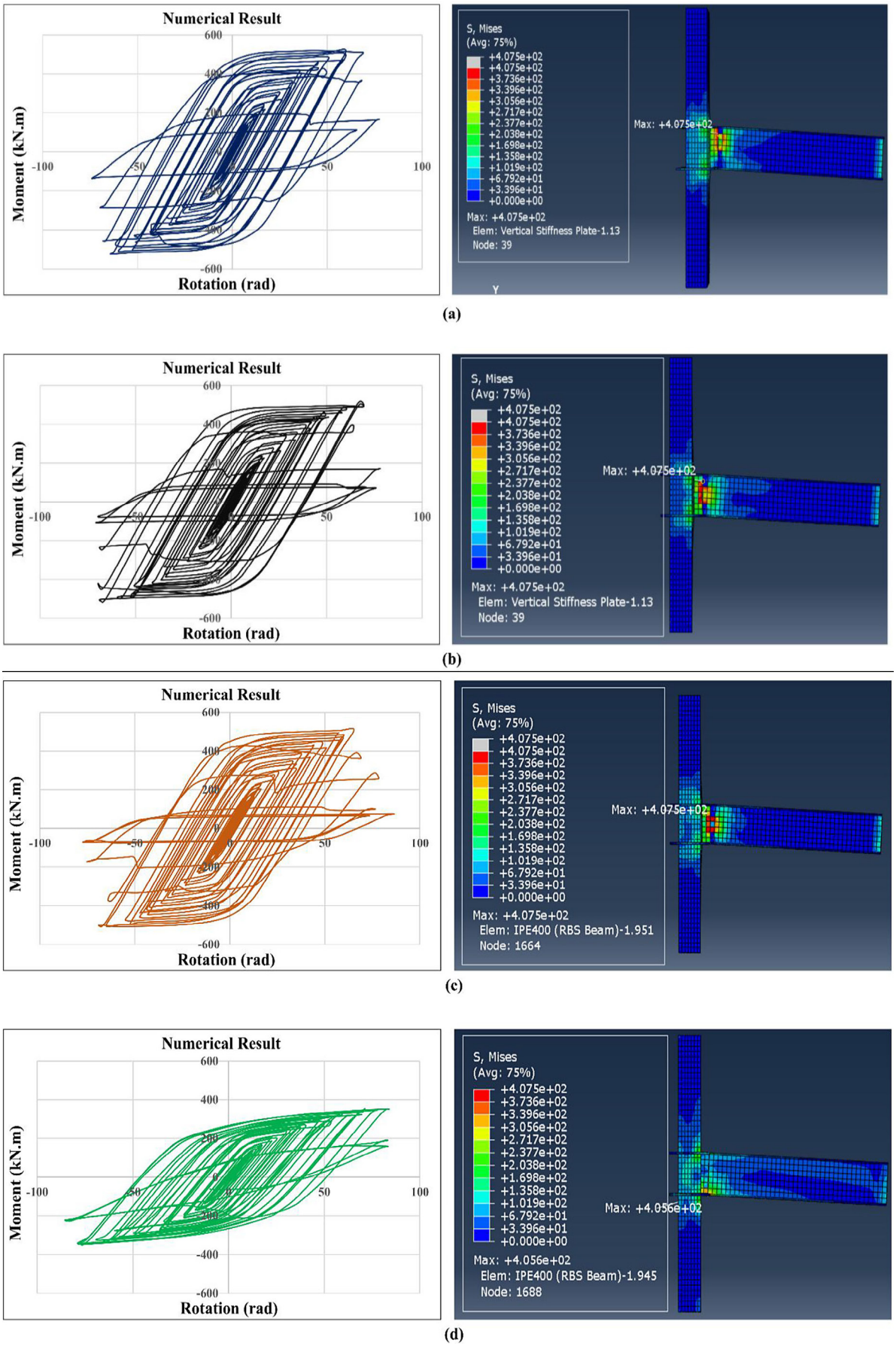

Figure 6. Von Mises stress distribution, plastic hinge location, hysteresis curves, and torque for connection configurations: (a) G01-V10%, (b) G01-V25%, (c) G01-V50%, (d) G01-V100%

increases, the column transitions from a tensile yielding response to a compressive buckling behavior at the beam-column interface.

Given that the most favorable failure mode in steel beam-to-column connections is cross-sectional yielding under tensile forces, these findings suggest that employing double-skin composite columns (DSCFT) enhances the seismic performance by promoting ductile failure mechanisms. Thus, controlling the void ratio within the column core plays a critical role in optimizing the seismic behavior of such composite systems.

Figure 7 presents the maximum tolerable moment for the first group of models, where the beam is connected to the two-layer composite DSCFT column. These maximum moment values were derived from the hysteresis diagrams of the numerical models. As it was shown in Figure 7, the highest moment corresponds to the G01-V10% model, while the lowest is associated with the reference model G01-V100%. Notably, all models featuring the double-skin DSCFT column cross-section exhibited higher maximum moment capacities compared to the reference model.

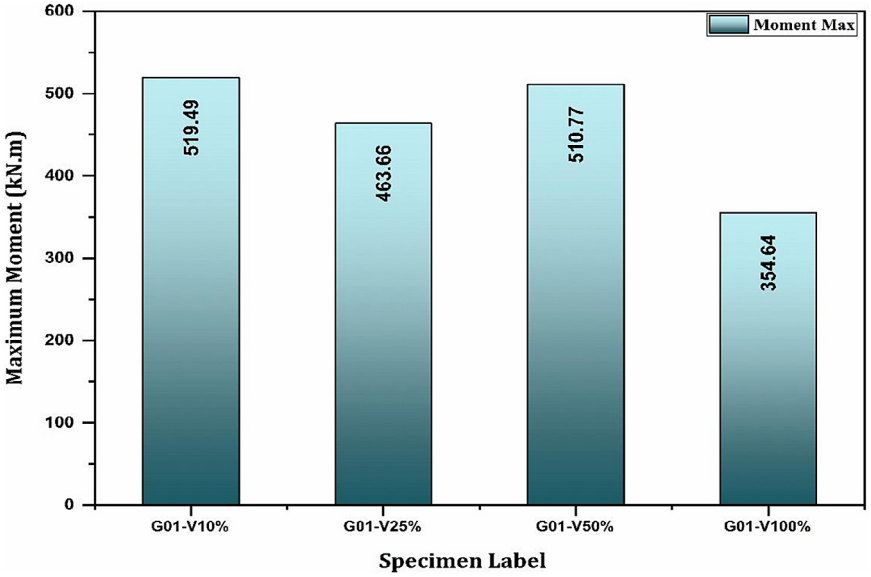

Figure 7. Maximum tolerable moment by beam to the DSCFT column in the first group

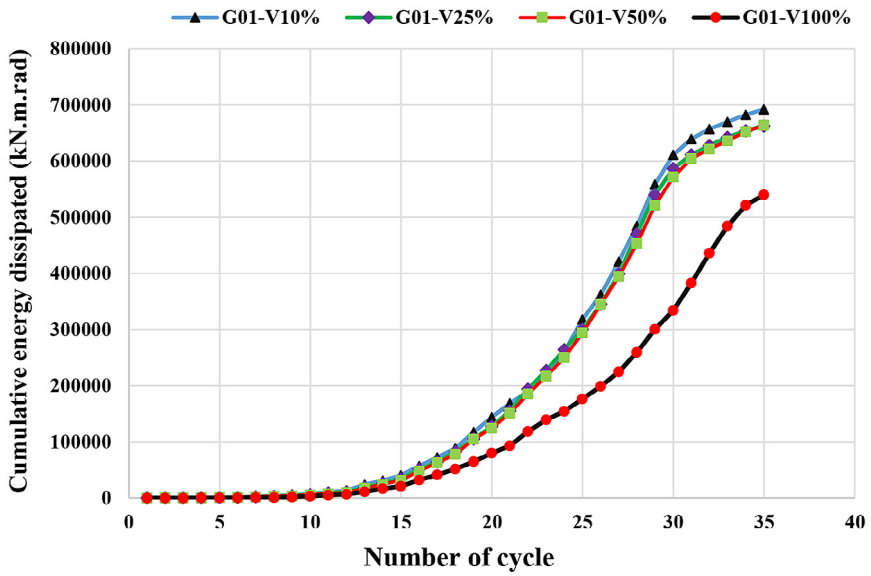

Figure 8. Cumulative dissipated energy for the first group

Another crucial factor in assessing seismic performance is the energy dissipation capacity. The structures with greater energy dissipation capability tend to demonstrate improved behavior during seismic events, enhancing overall resilience.

Figure 8 shows the cumulative energy dissipation results for the first group, which were calculated from as the area enclosed by the hysteresis loops for each loading cycle, which is equivalent to integrating the load–displacement curve over each cycle. This method allows for an accurate estimation of the energy dissipated during cyclic loading. The highest cumulative energy dissipation was observed in the G01-V10% model, while the lowest was recorded for the reference model (G01-V100%). The cumulative energy values for the G01-V25% and G01-V50% models are nearly identical. Overall, the results indicate that the use of double-skin composite (DSCFT) columns enhances energy dissipation across all models. However, increasing the percentage of voids within the column core reduces the amount of dissipated energy.

Investigation of the effect of concrete strength

One of the key factors influencing the seismic behavior of structures is the concrete strength. Since this factor has not been extensively studied in previous research, the present study investigated the effect of concrete strength on the behavior of double-skin composite DSCFT columns. For this purpose, the second group of models, detailed in Table 1, was analyzed and their results compared.

To identify the damage locations in the connection and assess seismic behavior, stress contours (S-contours) and time-period diagrams were utilized for the numerical models of the second group, as shown in Figure 9.

According to Figure 9, the reference model (G01-V100%) exhibits high stress concentration around most of the column area, indicating that the plastic hinge has shifted from the beam to the column, with maximum tension observed at the beam-column connection. Moreover, as concrete strength increases, the area subjected to maximum stress within the column decreases. Therefore, it can be concluded that increasing concrete strength in DSCFT sections enhances column stiffness, resulting in reduced stress and consequently less damage in the column.

In Figure 10, the maximum tolerable moment is shown by connecting the beam to the two-layer composite column DSCFT for the second group. As in the previous group, the maximum moment values are obtained from the hysteresis diagram of numerical models.

According to Figure 10, the lowest tolerable moment is related to the reference model (G01-V100%) and the highest tolerable moment is related to the G02-Fc70 model in which the concrete with a strength of 70 MPa is used. In which the cross-section of the composite column of the two skins is used, it can be concluded that increasing the strength of concrete has no significant effect on the maximum tolerable moment by connecting the beam to the column.

Figure 11 presents the cumulative dissipated energy diagram used to assess the effect of concrete strength on the seismic behavior of the beam-to-double-skin composite column connection. As illustrated, the lowest cumulative dissipated energy corresponds to the reference model (G01-V100%), while the highest is observed in the G02-Fc70 model. Moreover, the results indicate that increasing concrete strength leads to a corresponding increase in cumulative dissipated energy.

Investigation of the effect of inner skin thickness

Another important factor influencing the seismic behavior of steel beam connections to double-skin composite columns is the thickness of the inner steel tube. To investigate this effect, the models listed in Table 1 were developed and analyzed using the Abaqus software.

Figure 12 presents the stress distribution, locations of plastic hinge formation, and the moment-rotation hysteresis curves for these models. In the reference model (G01-V100%), the majority of the plastic deformation concentrates around the column, indicating a shift of the plastic hinge from the beam to the column. However, as the thickness of the inner skin increases, a larger portion of the plastic deformation occurs within the beam itself. This behavior suggests that increasing the inner skin thickness enhances the stiffness of the column, thereby promoting the formation of plastic hinges in the beam rather than in the column.

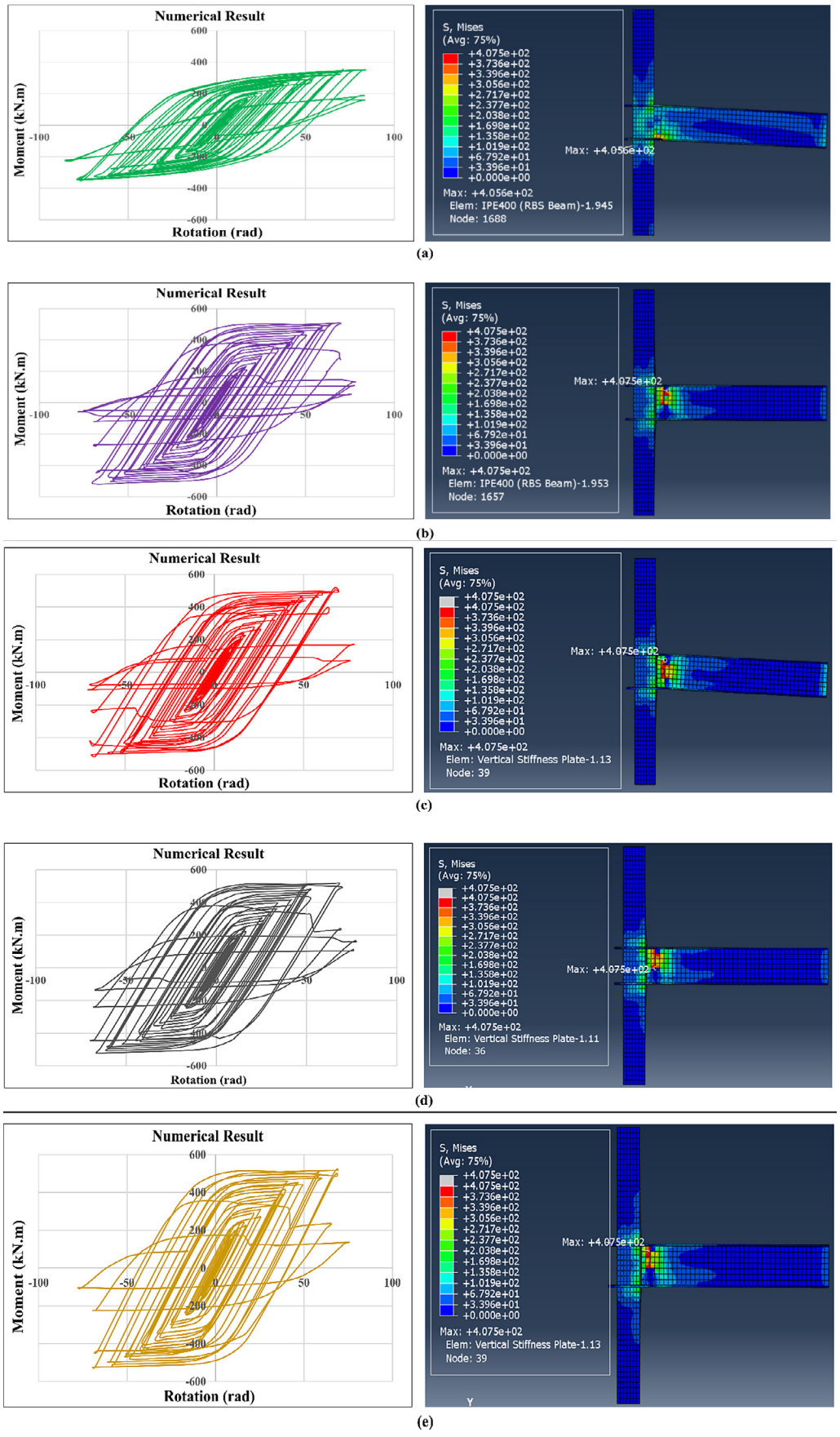

Figure 9. A picture of the von Mises stress distribution, and the formation location of the plastic hinge hysteresis curves and rotation torque for connection configurations: (a) G01-V100% – reference, (b) G02-Fc20, (c) G02-Fc30, (d) G02-Fc50, (e) G02-Fc70

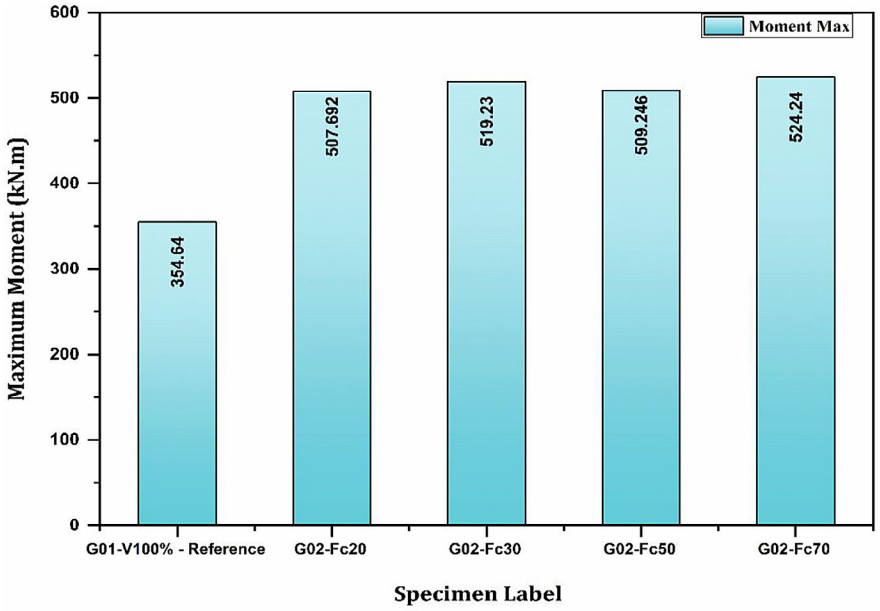

Figure 10. Maximum tolerable moment by connecting the beam to the composite column of two skins for the second group

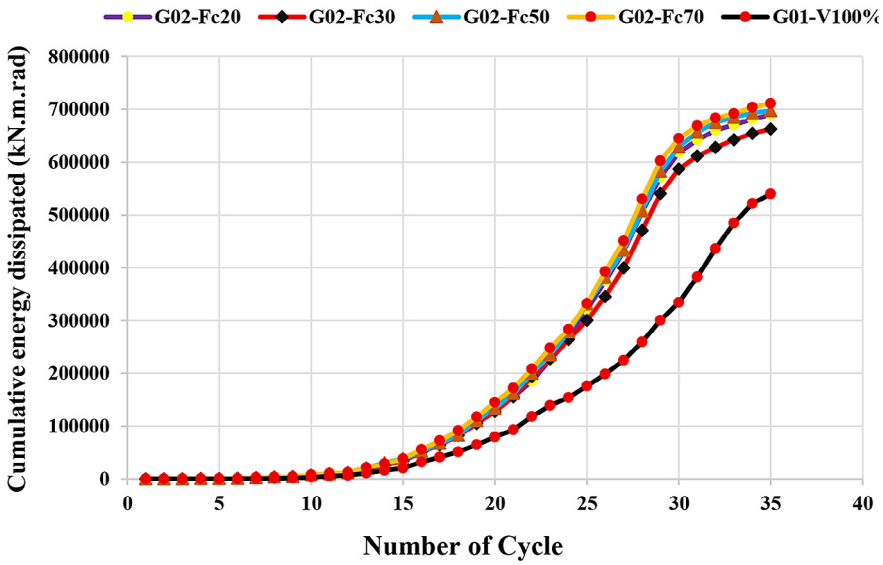

Figure 11. The effect of concrete strength on the energy dissipated by connecting the beam to the composite column of two skins

These findings highlight the critical role of inner skin thickness in controlling the failure mechanism and improving the seismic performance of double-skin composite columns.

On the basis of the hysteresis diagram shown in Figure 12, the maximum moment capacity when connecting the beam to the column is determined, as illustrated in Figure 13. According to Figure 13, the numerical model G03-IS15 has the highest tolerable moment, while the reference model (G01-V100%) has the lowest tolerable moment. In other words, by increasing the thickness of the inner skin from 5 to 15 mm, the maximum tolerable moment value increased from 506.978 to 520.892 kN.m.

Figure 14 shows the graph of cumulative dissipated energy in each cycle for the numerical models. Interestingly, the cumulative dissipated energy in the final cycles is highest for the model with an inner skin thickness of 5 mm and lowest for the reference model. This indicates that the thinner inner skin (5 mm) provides

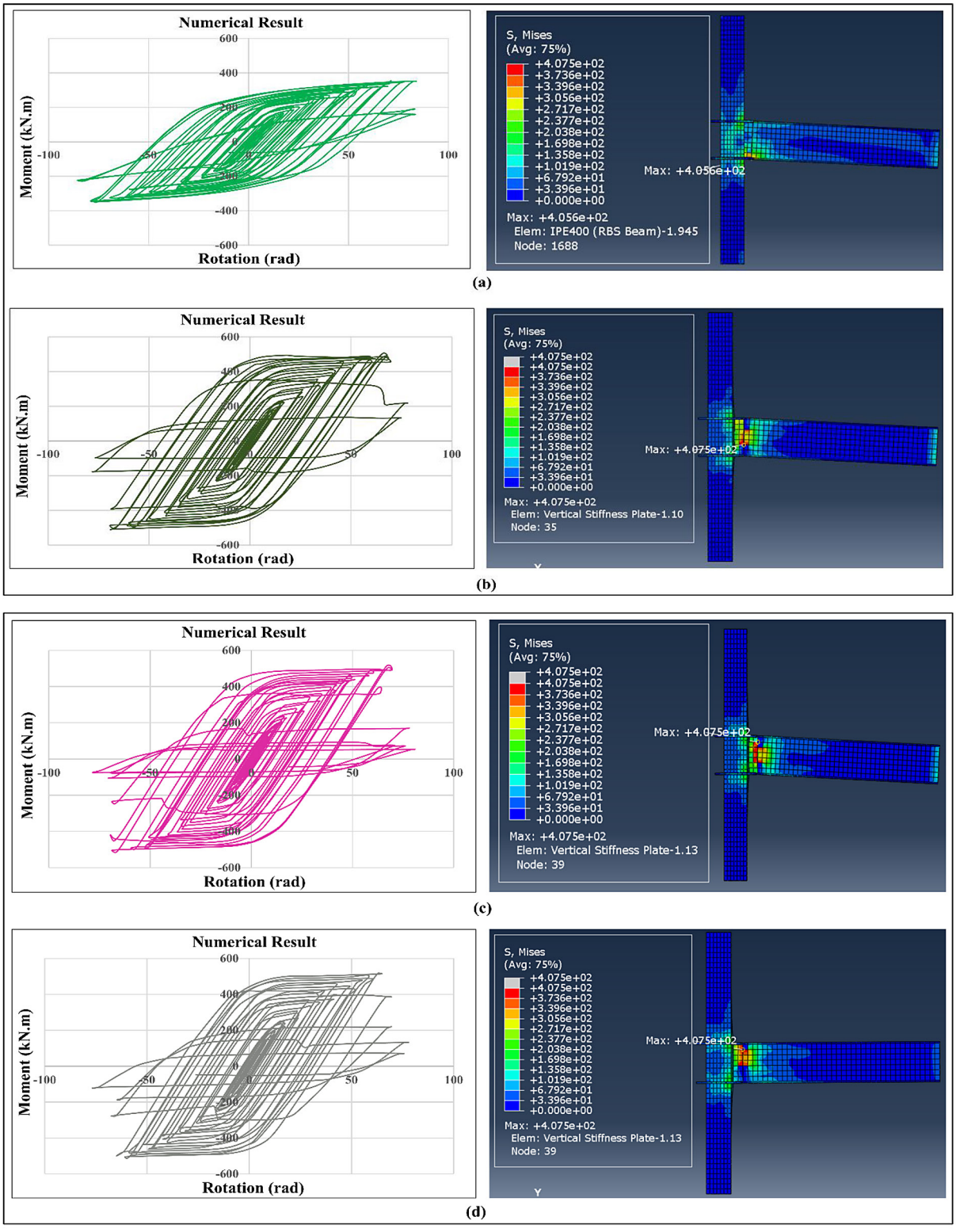

Figure 12. A picture of the von Mises stress distribution, and the formation location of the plastic hinge hysteresis curves and the rotation torque for connection configurations: (a) G01-V100%, (b) G03-IS5, (c) G03-IS10, (d) G03-IS15

higher ductility, whereas increasing the thickness enhances moment capacity. Therefore, selecting the inner skin thickness involves a balance between maximizing energy dissipation and achieving higher moment resistance. This clarification has been added to better highlight the relationship between inner skin thickness, ductility, and seismic performance.

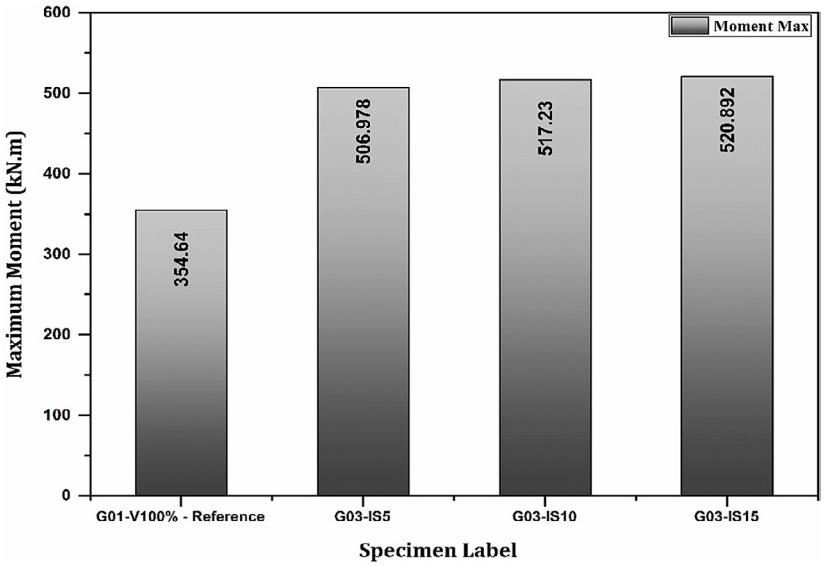

Figure 13. Maximum tolerable moment value for group III numerical models

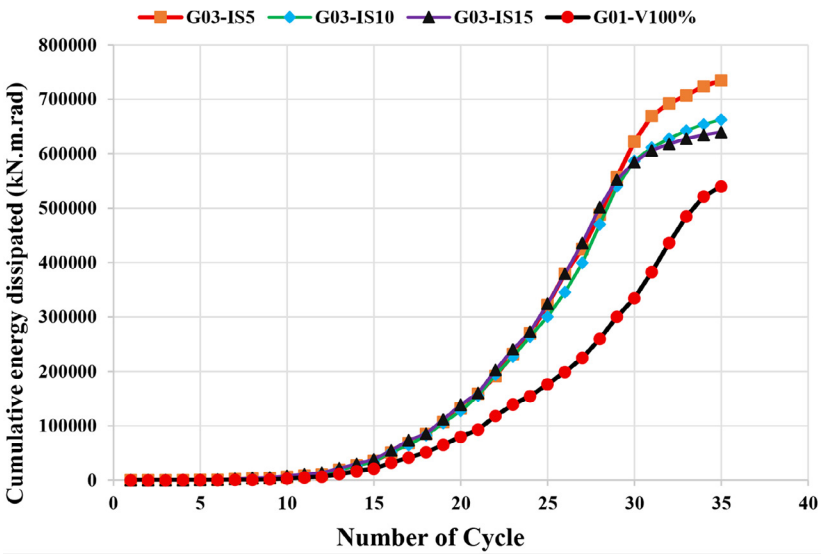

Figure 14. Cumulative dissipated energy for Group III numerical models

CONCLUSIONS

One of the types of connections is the connection of the beam to the DSCFT column. The main purpose of this study was to investigate the factors affecting the seismic behavior of the connection of the beam to the DSCFT column. The parameters studied in this study are the percentage of void in the middle of the column section, the compressive strength of the concrete, and the thickness of the inner skin. Three numerical model groups have been analyzed. The results of this research are summarized as follows.

1. With the increase in the void percentage, the rupture mode has changed from the state of cross-section flow due to tensile force to the buckling state of the section due to compressive force. Because the best rupture mode for connecting the beam to the DSCFT column is flow due to tensile force, because it will increase energy dissipation, and also the worst rupture mode is buckling due to compressive force, so it can be concluded that the use of DSCFT cross-section to normal sections, will improve the performance of fittings in steel structures.
2. By increasing the percentage of the void in the middle of the column from 10 to 100%, the maximum tolerable moment has decreased from 519.49 to 354.64 kN.m. Also, the cumulative dissipated energy has been drastically reduced.

3. Increasing the strength of concrete from 20 to 70 MPa has increased the maximum tolerable moment from 507.698 to 524.24 kN.m. Also, by increasing the strength of concrete, the cumulative energy of connecting the beam to the column has increased. In other words, according to the results of this study, it seems that the concrete in the DSCFT column has more role in preventing buckling. It is intolerable, but it has improved the accumulated spent energy.
4. In the reference model (G01-V100%), most of the area around the column has been stressed, which indicates that the plastic connection is being transferred from the beam to the column. By increasing the strength of concrete from 20 to 70 MPa, less part of the column is under stress, and more in the life of the beam and near the connection, the maximum stress is observed.
5. By increasing the thickness of the inner skin from 5 to 15 mm, the maximum tolerable moment has increased from 506.978 to 520.892 kN.m. Therefore, according to the results of this study, it is recommended that the thickness of the inner skin should be about 5 to 10 mm in the connection of the beam to the DSCFT column.
6. Increasing the thickness of the inner skin will have a great impact on the formation of plastic hinges in the beam, because it will increase the stiffness of the column. Also, increasing the thickness of the inner skin has caused a decrease in the cumulative dissipated energy in the final cycles and a decrease in the ductility of the beam-column connection.

Practical recommendations based on the study results:

- Void percentage in column core (~10%): Maintaining a low void ratio enhances the moment capacity and energy dissipation of a column, and promotes the formation of desirable plastic hinges in the beam, thereby improving seismic performance.
- Concrete compressive strength: Increasing concrete strength improves column stiffness, reduces high-stress regions, and enhances cumulative energy dissipation, resulting in superior seismic performance.
- Inner steel skin thickness: Increasing the inner skin thickness from 5 to 15 mm enhances column stiffness and maximum moment capacity, while thinner inner skins (5–10 mm) provide greater ductility during later loading cycles.
- Use of DSCFT: These columns promote ductile failure mechanisms and significantly increase energy dissipation capacity, making them effective for improving seismic resistance.
- Design optimization: Combining a low void ratio (~10%), high-strength concrete (≥50 MPa), and moderate inner steel thickness (5–10 mm) provides optimal seismic performance and efficient energy absorption.
- Structural applications: The DSCFT column system is well-suited for use in seismically active regions, offering enhanced ductility, lateral stability, and delayed local buckling.
- Construction feasibility: Double-skin systems reduce the overall structural weight while maintaining strength, making them practical for high-rise buildings and bridge columns.

Future work:

- Experimentally validate full-scale DSCFT beam–column connections under cyclic and dynamic loads.
- Investigate the influence of welding methods and connection details on local stress transfer.
- Explore the long-term performance and fatigue behavior under repeated seismic actions.
- Extend the analysis to multi-story frames to assess the global seismic performance of DSCFT-integrated systems.

Acknowledgements

The authors express their gratitude to the department head and staff of the Civil Engineering Department at the University of Babylon for their provision of facilities, which greatly contributed to the completion of this work.

REFERENCES

1. Sharmila S., Carm A. M., and Praveenkumar S., Axial performance of concrete-filled double skin hybrid tubular columns: Role of shear connectors and confinement rings, Iranian Journal of Science and Technology, Transactions of Civil Engineering, 2025; 49, 4691–4711.
2. Deng R., Zhang Z., and Xiang Y., Load-carrying mechanism of thin-walled hybrid double-skin tubular columns subjected to axial compression, Engineering Structures, 2025; 326, 119557.

3. Moradi R. and Khalilzadeh Vahidi E., General study of new ideas and practical of friction dampers for passive vibration control of structures, Karafan Journal, 2021; 17(4), 239–257.
4. Al Mashhadani D. A., Wong L. S., Al-Zand A. W., and Kong S. Y., Evaluating axial strength of cold-formed C-section steel columns filled with green high-performance concrete, Civil Engineering Journal, 2024; 10, 271–290.
5. Khalilzadehvahidi E., Khalil Zadeh Vahidi P., and Moradi R., Performance Pathology of Historic Adobe Structures and Their Methods of Retrofitting, Karafan Journal, 2019; 16(1), 53–66.
6. Owaid A. M., Akhaveissy A. H., and Al-Abbas B. H., Retrofitting seismically designed exterior beam-column joints under lateral monotonic loading: A numerical analysis based on experimental testing, Journal of Rehabilitation in Civil Engineering, 2026; 14(1).
7. [7] Kumar P. P. S. A. I., Singh S. B., Barai S. V., State-of-the-art review on axial behavior of frp-concrete-steel double-skin tubular columns, Indian Concrete Journal, 2025; 99(2), 48–63.
8. Wang J. J., Wang Z. C., Yu T., Nie X. F., and Zhang S. S., Behavior of FRP-UHPC-steel double-skin tubular columns under eccentric compression, Journal of Building Engineering, 2025; 108, 112884.
9. Mohammed A., Syamsir A., Lateef A., and Algaifi H., Performance of concrete-filled double-skin steel tube columns: A critical review of weaknesses and solutions, Engineering, Technology & Applied Science Research, 2025; 15(3), 23767–23776.
10. Mohammed Al-Araji A., Moradi R., and Mohammed Owaid A., Numerical investigation of bearing capacity and lateral response of pile group considering soil interaction, Salud, Ciencia y Tecnología - Serie de Conferencias, 2025; 4, 1582.
11. Abbood A. A. and Oukaili N., Behavior of axially loaded concrete columns reinforced with steel tubes infilled with cementitious grouting material, Civil Engineering Journal, 2024; 10(2), 599–613.
12. Abdulridha A. M. and Al Zaidee S. R., Experimental and numerical investigation of concrete-filled tube beams: A review paper, Journal of Engineering, 2025; 31(3), 18–41.
13. Moradi R. and Khalilzadeh Vahidi E., Comparison of numerical techniques of masonry infilled rc frames for lateral loads, Journal of Concrete Structures and Materials, 2018; 3(2), 102–118.
14. Chepurnenko A., Al-Zgul S., and Tyurina V., Machine learning for predicting required cross-sectional dimensions of circular concrete-filled steel tubular columns, Buildings, 2025; 15(9), 1438.
15. Zhu H., Ahmed M., Li C., et al., Fire resistance of square double-skin concrete-filled steel tubular columns and concrete-filled double steel tubular columns, Engineering Structures, 2024; 319, 118882.
16. Wang Z., Chen J., and Zhang R., Manuscript title: Experimental investigations of concrete-filled double skin steel tube column-column grouted connection under axial compression, Construction and Building Materials, 2024; 453, 138972.
17. Vahidi E. K. and Moradi R., Numerical study of the force transfer mechanism and seismic behavior of masonry infilled RC frames with windows opening, Civil Engineering Journal, 2019; 5(1), 61–73.
18. Wang C., Li S., Zhang Z., et al., Seismic behavior of concrete-filled double steel-plate composite walls with discontinuous internal steel plates: An experimental study, Construction and Building Materials, 2025; 489, 142361.
19. Fan J., Xie M., Liu Y., Guo H., and Zhao J., Seismic and numerical investigation of semi-rigid CFDST joints with flush endplates, Journal of Building Engineering, 2025; 102, 111983.
20. Moradi R. and Khalilzadeh Vahidi E., Experimental study of rotational-friction damper with two slip load and evaluation of its performance in RC frame under cyclic loading, Journal of Concrete Structures and Materials, 2021; 6(1), 121–137.
21. Hassan M. M., Mahmoud A. A., and Serror M. H., Behavior of concrete-filled double skin steel tube beam-columns, Steel and Composite Structures, 2016; 22(5), 1141–1162.
22. Zhang D., Zhao J., and Zhang Y., Experimental and numerical investigation of concrete-filled double-skin steel tubular column for steel beam joints, Advances in Materials Science and Engineering, 2018; 1, 6514025.
23. Hu Y., Zhao J., Zhang D., and Li Y., Cyclic performance of concrete-filled double-skin steel tube frames strengthened with beam-only-connected composite steel plate shear walls, Journal of Building Engineering, 2020; 31, 101376.
24. Zhou F., Li Y., and Dong B., Experimental investigation of concrete-filled double-skin stainless steel tubular beam-columns, Journal of Constructional Steel Research, 2022; 196, 107406.
25. Phan D. H. H., Patel V. I., Liang Q. Q., Al Abadi H., and Thai H.-T., Numerical investigations of circular double-skin steel tubular slender beam-columns filled with ultra-high-strength concrete, Engineering Structures, 2022; 254, 113814.
26. Vulcu C., Stratan A., Ciutina A., and Dubina D., Beam-to-CFT high-strength joints with external diaphragm. I: design and experimental validation, Journal of Structural Engineering, 2017; 143(5), 4017001.
27. Lemaitre J., A course on damage mechanics. Springer science & business media, 2012.

28. Sathe P. D. and Dawari B. M., Elasto-plastic damage analysis based on strain-space plasticity, Procedia Engineering, 2017; 173, 1108–1115.
29. Kim M.-S., Cho, Y.-H. and Jang H., Numerical modeling of stress-state dependent damage evolution and ductile fracture of austenitic stainless steel, International Journal of Solids and Structures, 2025; 318, 113439.
30. Santos R. O., Coelho P. de P., Vincze G., et al., Experimental–numerical investigation of the ductile damage of TRIP 780 steel, Metals, 2025; 15(9), 991.
31. Özkılıç Y. O., Investigation of the effects of bolt diameter and end-plate thickness on the capacity and failure modes of end-plated beam-to-column connections, Research on Engineering Structures & Material, 2021; 7(3), 445–463.
32. Lubliner J., Oliver J., Oller S., and Oñate E., A plastic-damage model for concrete, International Journal of Solids and Structures, 1989; 25(3), 299–326.
33. Jeeho L. and F. G. L., Plastic-damage model for cyclic loading of concrete structures, Journal of Engineering Mechanics, Aug. 1998; 124(8), 892–900.
34. ANSI/AISC 341-10, Seismic Provisions for Structural Steel Buildings, American Institute of Steel Construction, 2010.